Zero-temperature spin-wave damping in a spin-polarized Fermi liquid

Sorin Perisanu and Gerard Vermeulen*
Centre de Recherches sur les Très Basses Températures, CNRS, Boîte Postale 166, 38402 Grenoble Cédex 9, France
(Received 14 April 2006; published 19 June 2006)

We have measured the temperature and polarization dependence of the spin-wave damping and spin diffusion coefficient in a saturated ^{3}He-^{4}He mixture with a concentration of 9.4% at a pressure of 8 bars. A Leiden dilution refrigerator has been used to enhance the nuclear polarization and to cool the mixture to temperatures in the range 10–15 mK. The maximum polarization is 3.4 times higher than the equilibrium value of 2.7% in an external magnetic field of 11.36 T. The effects of the dipolar interactions and the radiation damping have been taken into account in the analysis of the spin-wave spectra. We observe that the polarization dependence of the spin-wave damping is proportional to $T^2+\mathcal{A}^2T_{a0}^2$ where T is the temperature, $\mathcal{A}$ is the polarization enhancement factor, and T_{a0} is the anisotropy temperature for the mixture at equilibrium in the external field. Our result $T_{a0}=3.66\pm0.14$ mK is 30% higher than the theoretical prediction for very dilute mixtures and is evidence for the existence of polarization-induced relaxation of transverse spin currents.

DOI: 10.1103/PhysRevB.73.214519 PACS number(s): 67.65.+z, 67.57.Lm, 67.60.−g, 71.10.Ay

I. INTRODUCTION

Each transport property in a degenerate Fermi liquid is governed by a relaxation time that is the result of scattering between quasiparticles. The Pauli exclusion principle restricts the phase space available for scattering to a shell of width k_BT around the Fermi surface, because only the quasiparticles in the shell can conserve energy and momentum during collisions. Consequently, the relaxation time is proportional to $1/T^2$, leading to a temperature dependence of the viscosity $\eta\propto 1/T^2$ and the thermal conductivity $\kappa\propto 1/T$. This remains true in a spin-polarized Fermi liquid with two Fermi distributions and different Fermi energies E_F^+ and E_F^- for particles with up and down spin as long as the relaxation time is determined by the collisions of quasiparticles in the thermal vicinity of the Fermi surfaces.

Theoretical study of the spin dynamics of Fermi liquids with arbitrary polarization led to the notion of anisotropic spin transport[1]. Transport in response to a perturbation of the amplitude of the magnetization is still controlled by a relaxation time $\tau_\parallel\propto 1/T^2$ because it involves only states near the two Fermi surfaces. In contrast, scattering in response to a perturbation of the direction of the magnetization can occur in all phase space between the Fermi surfaces E_F^+ and E_F^-. Therefore, the transverse relaxation time $\tau_\perp$ becomes polarization dependent and behaves in first approximation like $\tau_\perp\propto 1/(T^2+T_{a0}^2)$ where the anisotropy temperature T_{a0} is proportional to the gap $E_F^+-E_F^-$. Transverse spin dynamics is damped, because $\tau_\perp$ is finite at $T=0$ K.[2–4] The theoretical prediction for very dilute mixtures is $T_{a0}/B_0=\hbar\gamma/2\pi k_B=248\ \mu\mathrm{K}/T$, where B_0 is the applied magnetic field and γ the gyromagnetic ratio of ^{3}He.[2,4–6] The anisotropy temperature measured in interacting Fermi systems may depend strongly on Fermi liquid parameters which are not easily accessible.[3]

Conversely, Fomin[7] has argued that the magnitude of the local spin density is a conserved quantity and that the local spin density and the Landau field precess together. If the variations of the Landau field are slow and have a small amplitude, they can be treated as an adiabatic perturbation and do not give rise to scattering. He used a Langrangian in a reference frame tied to the oscillating magnetization to derive a spin-wave dispersion relation at $T=0$ K, which contains no damping up to second order in the wave vector. Fomin's work has been questioned by Mullin and Ragan[8] who derived the spin-wave dispersion relation from the kinetic equation in the same rotating frame as Fomin to show that it contains damping because of collisions between up- and down-spin quasiparticles. This work has led Fomin to reconsider the problem and he is convinced now that zero-temperature spin-wave damping does exist.[9] Mineev[10] has also argued that Fomin overlooked collisions between quasiparticles which introduce a finite imaginary self-energy part[11] in the Green's function for a polarized Fermi liquid and which inevitably lead to spin-wave damping.

Magnetization transport in polarized Fermi liquids depends on gradients in the amplitude and the direction of the magnetization. Letting $\nabla\mathbf{M}=\hat{\mathbf{e}}\nabla M+M\nabla\hat{\mathbf{e}}$ with $|\mathbf{M}|=M$ and $\hat{\mathbf{e}}$ a unit vector in the direction of the magnetization, the magnetization current $\mathbf{J}$ can be written as[1,12]

$$J_j=-D_\parallel\frac{\partial M}{\partial r_j}\hat{\mathbf{e}}-\frac{D_\perp}{1+(\mu M)^2}\left(M\frac{\partial\hat{\mathbf{e}}}{\partial r_j}+\mu M^2\hat{\mathbf{e}}\times\frac{\partial\hat{\mathbf{e}}}{\partial r_j}\right). \quad (1)$$

The longitudinal and transverse spin transport are described by the first and second term on the right-hand side. The transverse spin diffusion constant is given by

$$D_\perp=\frac{v_F^2}{3}(1+F_0^a)\tau_\perp, \quad (2)$$

where v_F is the Fermi velocity and F_0^a a Fermi liquid parameter. Equation (1) is an extension of one of the Leggett equations[13] describing spin-waves and anomalous spin echo behavior (the Leggett-Rice effect) in Fermi liquids at higher polarizations. In the literature, one finds also another notation $\mu M=-\lambda\omega_0\tau_\perp$, where ω_0 is the Larmor frequency, and λ is defined in terms of the Fermi liquid parameters F_0^a and F_1^a as $\lambda\equiv(1+F_0^a)^{-1}-(1+F_1^a/3)^{-1}$.

Several measurements of the anisotropy temperature by spin-echo decay in pure ^{3}He (Refs. 14 and 15) and in

^{3}He-^{4}He mixtures[16–20] have been published with results ranging from one to ten times the dilute Fermi gas prediction. The experimental discrepancies have been explained in terms of effects mimicking an apparent T_{a0} such as restricted diffusion due to a finite sample size[21] or unstable growth of magnetization perturbations after imperfect rf pulses far in the collisionless regime or in the presence of a demagnetizing field. For instance, the discrepancy in the results for T_{a0}/B_0 in some ^{3}He-^{4}He mixtures have been attributed to restricted diffusion,[16,19] the discrepancies in pure ^{3}He may originate in demagnetizing field effects,[14,15] and the anomalous saturation of the spin rotation $|\lambda\omega_0\tau_\perp|$ to values less than 10 in very dilute mixtures has been tentatively ascribed to spin-wave instabilities.[18] To get rid of the latter instabilities, a beautiful spin-echo experiment resulting in a value for T_{a0}/B_0 close to the dilute gas prediction has been done at ^{3}He concentrations x_3 very near the critical concentration $x_c \approx 3.8\%$ at which the interaction parameter λ and $\lambda\omega_0\tau_\perp$ vanish.[20] An experiment has been reported to measure the anisotropy temperature by spin-wave damping[22] which did not have the sensitivity to distinguish between the dilute gas prediction and $T_{a0}=0$ K. However, it has cast a doubt on the rather high values for T_{a0} obtained in the spin-echo experiments preceding it.

Spectra of standing spin-wave modes can be created by trapping the spin-waves in a cavity formed by a magnetic field gradient and the walls of the experimental cell. Precise measurement of the damping requires spectra with well-separated and identified modes and therefore good control of the boundary conditions and the applied magnetic field gradients. Symmetry breaking by insufficient field shimming complicates the analysis of the spectra seriously, because each mode can break up in closely spaced modes with lower symmetry. Candela *et al.*[23] have used a spin-wave cavity with a spherical geometry to eliminate symmetry breaking due to misalignment of the magnetic field gradient. In comparison with spin-echo experiments, spin-wave experiments have te advantages of (1) being less sensitive to nonlinear behavior because the magnetization is always excited with a small angle and (2) measuring the individual localized modes instead of an integral of the magnetization over the sample. Therefore, the analysis of a spin-wave experiment exposes most defects and must be reliable once the experimental conditions are sufficient to obtain good fits of the observed spectra. History has shown that spin-echo experiments may give conflicting results even when the results look internally consistent.

In this paper, we present measurements of spin-wave damping in a saturated dilute ^{3}He-^{4}He mixture at a pressure of 8 bars using a hemispherical cavity in an external field of $B_0=11.36$ T. The spectra analyzed here have been obtained using a ^{4}He circulating dilution refrigerator to enhance the polarization by a factor $1<\mathcal{A}\equiv M/M_0<3.4$ with respect to its equilibrium value of 2.7% at temperatures in the range of 10–15 mK. Essential improvements with respect to the previous spin-wave experiment[22] are the quality of the spectra and the thermometry.

Nowhere in the derivation of the Leggett equations for spin dynamics at low polarization[13,24] and their extension to high polarization[24] has it been assumed that the deviation of M_z from its equilibrium value M_0 must be small. In addition, Meyerovich has given a general macroscopic derivation of a Leggett-like equation for a Fermi system with exchange interactions which covers equilibrium and nonequilibrium polarizations.[25] Consequently, the theoretical description is still valid for systems where the polarization has been enhanced by pumping techniques. Using the magnetization enhancement factor $\mathcal{A}\equiv M/M_0$, we write the Landau molecular field as $\lambda\mathcal{A}\omega_0$ instead of $\lambda\omega_0$ and approximate the relaxation time as $\tau_\perp \propto 1/(T^2+\mathcal{A}^2T_{a0}^2)$ to account for pumping.

A figure of merit indicating the suitability of an experiment for the determination of T_{a0} is the ratio $\mathcal{A}B_0/T$ which ranges from 8500 in the experiment by Akimoto *et al.*,[20] 3800 in the experiment by Buu *et al.*,[19] to 2700 in this work. However, our experiment results in smaller errors in $\lambda\tau_\perp$ and $D_\perp$ which compensate for the lower value of $\mathcal{A}B_0/T$.

II. CALCULATING THE SPIN-WAVE SPECTRA

In our experimental conditions, the motion of the transverse magnetization $M_+(\mathbf{r},t)=M_x(\mathbf{r},t)+iM_y(\mathbf{r},t)$ is affected not only by the spin transport described by the Leggett[13] theory, but also by the dipolar interactions between the ^{3}He nuclei. The evolution of the transverse magnetization obeys for small excitations ($M_+ \ll M_z$) the following linearized equation of motion:[26]

$$i\frac{\partial M^+}{\partial t} = \frac{iD_\perp}{1+i\lambda\mathcal{A}\omega_0\tau_\perp}\nabla^2 M_+ + \omega_L(\mathbf{r})M_+ + \frac{\omega_M}{2}\{(1-2\hat{n}_{zz}[1])M_+ - \hat{n}_{zz}[M_+]\}. \quad (3)$$

The first term on the right-hand side arises from the dissipative and reactive spin currents following from Eq. (1). The second term describes the Larmor precession in the applied magnetic field. The third term is due to the demagnetizing field and exists also in classical systems. It gives rise to the appearance of magnetostatic or Walker modes, an effect which is also known as spectral clustering.[27–29] Here, $\omega_M \equiv 4\pi\gamma M$ with γ the gyromagnetic ratio of ^{3}He, M is the magnetization, and

$$\hat{n}[f(\mathbf{r})] \equiv -\frac{1}{4\pi}\frac{\partial^2}{\partial z^2}\int \frac{f(\mathbf{r})}{|\mathbf{r}-\mathbf{r}'|}d^3\mathbf{r}'.$$

The geometry of the experimental cell is a hemisphere with a radius of 1 mm on top of a bigger cylinder with entrance and exit tubes and is described in detail in Sec. III. The parts of the spin-wave spectra analyzed in this paper are due to modes localized in a region against the top of the hemisphere with a thickness of 0.1 mm. The third term in Eq. (3) is nonlocal but as long as it is small, the modes in the region of interest are unaffected by the magnetization in the cell far from this region. Therefore, we approximate the experimental setup as a sphere with radius R and a magnetic field with a constant gradient in the z direction so that $\omega_L(\mathbf{r})=\omega_0+\gamma Gz$, where ω_0 is the Larmor frequency at the center of the sphere and $\gamma GR \ll \omega_0$. In this case, the contribution due the dipolar interactions in Eq. (3) simplifies, since for a sphere $1-2\hat{n}_{zz}[1]=1/3$:

$$i\frac{\partial M^+}{\partial t} = \frac{iD_\perp}{1+i\lambda\mathcal{A}\omega_0\tau_\perp}\nabla^2 M_+ + (\omega_0+\gamma Gz)M_+ + \frac{\omega_M}{2}\left(\frac{1}{3}M_+ - \hat{n}_{zz}[M_+]\right). \quad (4)$$

The solution of Eq. (4) with the boundary condition of zero spin current into the wall ($\nabla M_+ \cdot \mathbf{n}=0$) and with $\lambda\mathcal{A}\omega_0\tau_\perp$ or ω_M sufficiently large leads to a spectrum of well-separated modes. When the demagnetizing field can be neglected, the modes are standing Silin spin waves confined by the field gradient against the wall with a characteristic wavelength ξ given by[23]

$$\xi^3 = \frac{D_\perp}{\gamma G\lambda\mathcal{A}\omega_0\tau_\perp}.$$

The characteristic frequency scale $\delta\omega_{sw}$ of the Silin spin-wave modes is of order $\gamma G\xi$. The ratio $\omega_M/\delta\omega_{sw}$ parametrizes the importance of the dipolar interactions.[26] The nature of the modes is more Walker-like than Silin-like when $\omega_M/\delta\omega_{sw}>1$. In our experiment this ratio increases from 0.1 to 0.5 when the polarization enhancement factor $\mathcal{A}$ increases from 1 to 3.4. Therefore, our spectra are still Silin-like but the effect of the demagnetizing field cannot be neglected.

A brute force method to calculate the spectra is to find a solution of Eq. (4) in terms of a basis set formed by the solutions of the wave equation in spherical coordinates,[23,26]

$$M_+(\mathbf{r}) = \sum_{n=0}^{\infty}\sum_{l=0}^{\infty}\sum_{m=-l}^{m=l} c_{nl} j_l(k_{nl}r) Y_l^m(\theta,\phi). \quad (5)$$

Equation (5) is a solution of Eq. (3) without the gradient term and the demagnetizing field. The wave numbers k_{nl} are determined from the boundary condition: $k_{nl}R$ must be equal to the $(n+1)$th zero of the derivative of the spherical Bessel function $j_l(x)$. We restrict the basis set to functions with $m=0$, since only those couple to a homogeneous rf field. Substitution of Eq. (5) in Eq. (4) gives a non-Hermitian eigenvalue problem which can be solved to obtain the complex eigenvalues and eigenmodes of the spin-wave spectrum. The coupling of the modes with the transverse pulsed rf field allows one to calculate the weights of the modes. We refer to Appendix E of Krotkov *et al.*[26] for the derivation of the matrix elements; the matrix elements are given by Eq. (81), (82), and (84) of that paper.[26] In practice, the basis set has to be truncated to some $(n,l)<(n_{max},l_{max})$ and the accuracy of the method depends on the selected subset of basis functions and the ratio ξ/R. We have used real matrices with up to 31 360 000 elements ($n_{max}=40$ and $l_{max}=140$) and complex matrices with up 12 845 056 elements ($n_{max}=32$ and $l_{max}=112$) for values of ξ/R down to 0.02.

Figure 1 shows the effect of the demagnetizing field calculated by diagonalization on the spin-wave modes confined within a distance of $R/10$ from the top of the sphere. The parameters correspond to our experimental conditions. The relative positions of the modes are very sensitive to ξ/R, γGR, and corrections due to the dipolar interactions. Neglecting the dipolar interactions in our experiment leads to values for ξ/R that are more than 10% too small and a small but systematic decrease of the values for γGR with increasing polarization.[30]

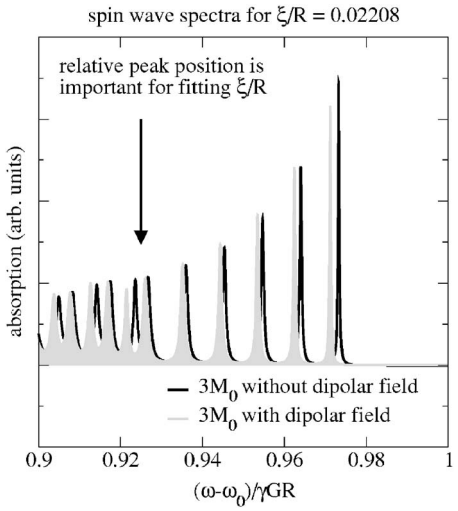

FIG. 1. Calculated effect of the demagnetizing field for a typical spectrum in a sphere. The normalized frequency $(\omega-\omega_0)/\gamma GR$ ranges from −1 at the bottom of the sphere to 1 at the top. The black and gray curves show calculations excluding and including the demagnetizing field respectively. The relative positions of the modes indicated by the arrow—(1,0) and (0,5)—and also their position with respect the first mode on the right—(0,0)—are very important for the determination of ξ/R and γGR. Interpretation of the experimental spectra without accounting for the demagnetizing field leads to values for ξ/R that are at least 10% too small.

The brute force method is too slow to fit the experimental spectra directly, because the numerical solution of the eigenvalue problem takes on order of 1 h on a fast personal computer. An approximate solution for the eigenfrequencies of the first modes of Eq. (4) neglecting the dipolar interactions can be found using the adiabatic approximation in the case that $\xi \ll R$.[26] The eigenfrequencies are given by

$$f_{nl} = \frac{\omega_{nl}-\omega_0}{\gamma R} = 1 + \frac{\xi}{R}\left(\alpha_{n+1} - \sqrt{\frac{2\xi}{R}}(2l+1)\right), \quad (6)$$

where the α_{n+1} are the $(n+1)$th zeros of the derivative of the Airy function. Equation (6) reduces to the solution of a one-dimensional spin wave problem in the limit $R\to\infty$. The adiabatic approximation helps to identify the modes in the spectra: n and l count the number of zeros of a mode in the directions parallel and perpendicular to the direction of the field gradient, respectively. Equation (6) allows one also to calculate the width of the modes after substituting ξ with $\zeta = \xi\sqrt[3]{1/(1-i/\lambda\mathcal{A}\omega_0\tau_\perp)}$ where we take the root closest to 1. We have verified that the relative difference in eigenvalues calculated by Eq. (6) and by the brute force solution of Eq. (4) without the dipolar interactions is less than 0.01% for the first 10–15 modes. We add a correction $a_{nl}+b_{nl}/\xi^3$ to each f_{nl} given by Eq. (6) to include the effect of the demagnetizing field. The values for a_{nl} and b_{nl} have been obtained by diagonalizing the eigenvalue problem Eq. (4) with and without the dipolar interactions for different values of $\mathcal{A}$ in the range $1\leqslant\mathcal{A}\leqslant 3$ and fitting the differences as a function of ξ.

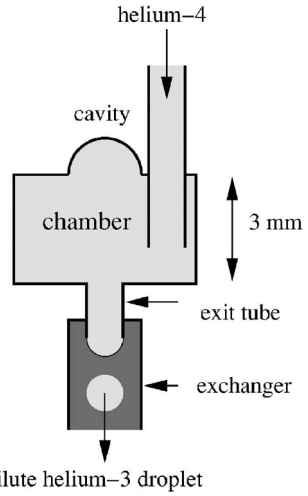

FIG. 2. The experimental chamber in operating conditions: dilute and concentrated ^{3}He are indicated by light and dark gray. The dilution process is maintained by injecting superfluid ^{4}He into the chamber to form dilute ^{3}He droplets at the exit tube. Concentrated ^{3}He enters the chamber after the injection of superfluid ^{4}He has been stopped. The spin-wave modes are confined against the top of the hemispherical cavity.

III. EXPERIMENTAL SETUP

The experiments have been performed on the dilute phase in the mixing chamber of a ^{4}He circulating dilution refrigerator. Diluting ^{3}He into ^{4}He in a magnetic field and at a pressure above 2.6 bars cools and enhances the nuclear polarization with respect to its equilibrium value.[31] The final polarization enhancement is obtained when the rate of polarization gain—roughly proportional to the circulation rate—equals the rate of polarization loss due to intrinsic or surface-induced relaxation processes. A maximum polarization enhancement factor of $\mathcal{A}=7$ has been reported in an external magnetic field of 7 T.[31] In the present experiment the relaxation time of the polarization is a factor 3–5 shorter and the polarization enhancement is limited to $\mathcal{A}<4.4$ in a magnetic field of 11.36 T. However, we present only data with $\mathcal{A}<3.4$ since they contain the highest values for $\mathcal{A}B_0/T$ and are unaffected by possible systematic errors in the ^{3}He concentration of the dilute phase due to the higher circulation rates needed to obtain the higher polarizations. The effect of the circulation rate on the ^{3}He concentration in the dilute phase will be estimated below.

Figure 2 shows the mixing chamber design adapted to spin-wave experiments in the dilute phase. The mixing chamber is assembled out of Araldite epoxy pieces, glued and coated with Stycast 1266 to obtain a smooth surface. The spin waves are observed in a hemispherical cavity which has been made by putting a little bit of Stycast 1266 in a $\oslash$ 2 mm hole and letting the capillary forces form a surface with a radius of 1 mm while the epoxy settles. The epoxy must settle at room temperature since the acceleration of the exothermic chemical reaction at higher temperatures amplifies temperature gradients and causes deformation of the surface. The relative error in the radius is estimated to be 5%. The cavity can be considered spherical for the modes of interest, since they are confined within a region of 0.1 mm height extending from the top of the cavity and die out exponentially toward the bottom.

The temperature is measured with a vibrating wire viscometer made out of a $\oslash$ 25.7 μm PtRh wire. We have found that ^{4}He preferentially absorbed on the wire may affect the viscosity measurements.[32] The slip length is normally on order of the mean free path but it is enhanced by two orders of magnitude for our PtRh viscometers in the dilute phase. The slip length may become larger than the diameter of the wire while the liquid is still in the hydrodynamic regime. The effect of the slip on a vibrating wire resonator has been calculated[33] and we find good agreement with this model.[34] We have used a melting curve thermometer to measure the temperature dependence of the viscosity between 10 and 100 mK at pressures ranging from 0 to 20 bars. Contrary to earlier work,[35] we obtain a viscosity η in the dilute phase which has a temperature dependence in agreement with the theoretically predicted leading-order finite-temperature correction: $1/\eta T^2=a-bT$.[36,37] We expect the viscosity to increase by 2–3 % for a change in polarization from 0 to 10% on the basis of measurements of the polarization dependence of the viscosity in pure ^{3}He.[38,39] Since the corresponding temperature decrease is barely visible in our data, we do not take into account the polarization dependence of the viscosity.

The diameter of the exit tube is chosen such that the concentrated phase cannot enter the chamber when superfluid ^{4}He is injected into the chamber. The dilution process takes place at the interface between the two phases at the bottom of the exit tube where dilute droplets are formed. The mixture in the chamber is cooled and polarized by heat and spin transport through the exit tube. Mutual friction between the superfluid ^{4}He flowing through and the ^{3}He atoms at rest inside the exit tube can decrease the ^{3}He concentration in the chamber with respect to saturation concentration at the interface. We evaluate the concentration decrease to be 2×10^{-5} for a saturation concentration of 6.6×10^{-2} at a pressure of 0 bar using Eq. (30) of Castelijns *et al.*[40] Therefore, mutual friction will not affect our experiment either at the working pressure of 8 bars.

The osmotic pressure depends on temperature and concentration and is conserved in ^{3}He-^{4}He mixtures in the absence of mutual friction. Therefore, it relates a temperature difference between the liquid in the chamber and the interface to a concentration difference. This effect is known as the heat flush effect. We believe that the temperature at the interface can be as low as 7 mK, because we have measured 7 mK in chambers with a different geometry where the concentrated phase and the phase separation interface sit inside the chamber. We evaluate a concentration decrease of 2×10^{-4} for a saturation concentration of 6.6×10^{-2} and a temperature difference from 0 to 15 mK at a pressure of 0 bar based on the data by Kuerten *et al.*[41] This effect is comparable at higher pressures since the calculation involves thermodynamic quanties which are weakly pressure dependent. Therefore, we present only data obtained with the lower circulation rates with $T<15$ mK and a polarization gain $\mathcal{A}<3.4$.

The chamber is surrounded by a birdcage resonator with a diameter of 11.5 mm and six inductive rungs with a length of

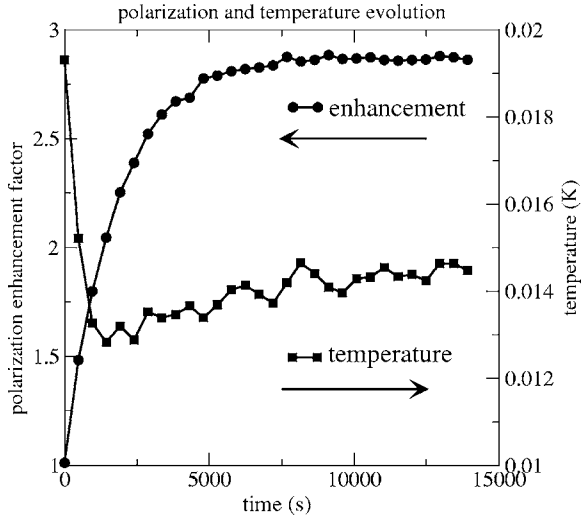

FIG. 3. The evolution of the temperature and polarization in the mixing chamber.

12 mm.[42] The resonator is tuned to a resonance frequency of 368.4 MHz at an impedance of 50 Ω and it has a quality factor of order 100. The NMR spectrometer allows one either to measure the full NMR spectrum by sweeping the frequency over the cell or to zoom in on the spin-wave modes by low-power pulsed NMR with an estimated tipping angle of 5° for a pulse length of 100 μs.

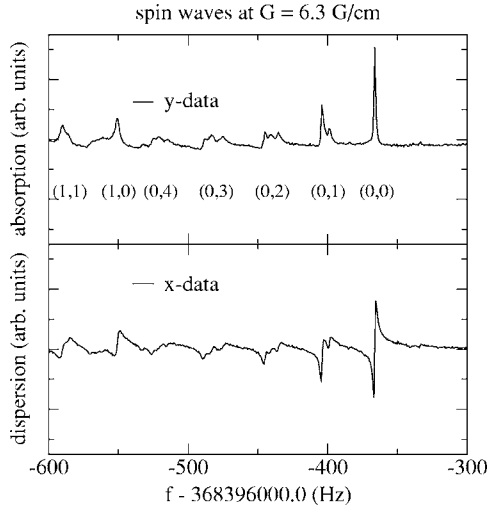

FIG. 4. A spin-wave spectrum at a gradient of 6.3 G/cm: 4.1 G/cm is due to the intrinsic inhomogeneity of the main 12 T coil and 2.2 G/cm has been applied with the gradient coil. The splitting of the modes with quantum numbers $(n,l)=(0,1),(0,2),(0,3),\ldots$ makes it difficult to fit the spectrum. We believe that the degeneracy of those modes has been lifted by imperfections in the applied magnetic field or in the wall of the spin-wave cavity. The modes with quantum numbers $(n,l)=(0,0),(1,0),\ldots$ do not show any lifting of degeneracy. The splitting of the modes with $l>0$ decreases with increasing field gradient and is barely visible at the highest field gradient as shown in Fig. 5.

IV. EXPERIMENTAL DATA AND ANALYSIS

A. Experimental data

Figure 3 shows the evolution of the temperature and the polarization enhancement factor in the dilute phase, shortly after the circulation of superfluid ^{4}He has been started. A pulsed NMR spectrum has been taken at each measurement of the temperature and the polarization. Concentrated ^{3}He fills the experimental cell and the magnetization relaxes to its equilibrium value after the circulation of superfluid ^{4}He has been stopped. The signal of the cell filled with concentrated ^{3}He at equilibrium is used to calibrate the sensitivity of the spectrometer in the continuous wave NMR mode. The pressure in the cell is 8 bars, because it is the best compromise between highest polarization and lowest temperatures. The ^{3}He saturation concentration is 9.4% and the equilibrium polarization in an external field of 11.36 T is 2.7%.

Figures 4 and 5 show spin-wave spectra at the minimum (6.3 G/cm) and maximum (23.7 G/cm) field gradient that we have applied. The field gradient contains a contribution of 4.1 G/cm due to the main field coil and a contribution from a gradient coil with a maximum gradient of 20.0 G/cm. The absorption peaks in the spectra have been labeled with the quantum numbers (n,l) belonging to Eq. (6). The modes in Fig. 4 with $(n,l)=(0,1),(0,2),(0,3),\ldots$ show a lifting of degeneracy which we ascribe to symmetry breaking by imperfections in the field gradient or the wall of the cavity. Figure 5 shows that increasing the applied field gradient suppresses the lifting of degeneracy to a large extent. Therefore, we have only analyzed the spectra at the highest applied gradient. We will use later that the modes with $(n,l)=(0,0)$ and (1,0) do not show any lifting of degeneracy, even at a field gradient of 6.3 G/cm.

The Appendix contains an estimate of the nonuniformity of the maximum magnetic field gradient from the line shape of the continuous-wave NMR spectra.

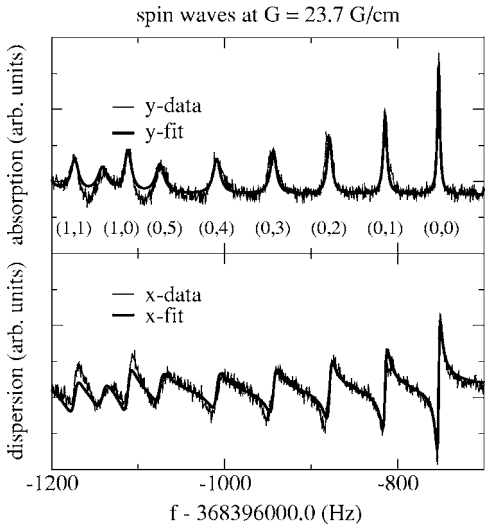

FIG. 5. A spin-wave spectrum at the maximum field gradient and a polarization enhancement factor of $\mathcal{A}=3.32$. The fine noisy curves are the experimental data and the thick smooth curves are a fit to modes shown. The lifting of degeneracy of modes with $l>0$ clearly visible in Fig. 4 is still present but barely visible. Therefore, we readjust the final value for $\lambda\mathcal{A}\omega_0\tau_\perp$ by interpolating only the first mode, keeping ξ/R and γGR constant.

B. Data analysis

Comparison of Fig. 1 with Fig. 5 shows that amplitude of the modes in the experimental spectra decreases somewhat faster with increasing l than the amplitudes of the modes in the calculated spectra. Therefore, we fit the spectra using a function that is based on Eq. (6) and includes the corrections $a_{nl}+b_{nl}/\xi^3$ to account for the dipolar field and a phenomenological formula for the amplitude of the modes.

All spectra have been interpolated by a complex function with ten real parameters. Three parameters—ξ/R, $\lambda\mathcal{A}\omega_0\tau_\perp$, and γGR—are related to the Silin spin-wave part of Eq. (4) and allow one to obtain the quantities of interest $\lambda\tau_\perp$ and $D_\perp$. The parameters ξ/R, $\lambda\mathcal{A}\omega_0\tau_\perp$, and γGR determine the position of the modes, the width of the modes, and the overall frequency extent of the spectrum. The other parameters account for experimental details: the frequency of the first resonance, a global phase factor to separate the absorption from the dispersion in the spectra, three parameters to characterize the amplitudes of the modes, and two baseline offsets.

Figure 5 shows a comparison of an interpolated spectrum and an experimental spectrum. In general, the positions of the modes in the experimental and interpolated spectra agree. However, the widths of the modes in the interpolated spectra with $(n,l)=(0,0)$ and (1,0) are too large. We explain this discrepancy by a degeneracy of the modes with $l>0$ which has been lifted by imperfections in the field gradient or in the wall of the spin wave cavity. The interpolation does not account for the lift of degeneracy and returns values for $\lambda\mathcal{A}\omega_0\tau_\perp$ which are too small. The experimental evidence in support of this explanation is illustrated by Figs. 4 and 5 showing that increasing the magnetic field gradient reduces the lifting of degeneracy of all modes except for the modes with $(n,l)=(0,0)$ and (1,0) which show no lifting of degeneracy. Therefore, we improve the values for $\lambda\mathcal{A}\omega_0\tau_\perp$ in an interpolation of the mode $(n,l)=(0,0)$ while keeping γGR and ξ/R constant. This readjustment increases the values for $\lambda\mathcal{A}\omega_0\tau_\perp$ by 10–20 %.

The rotating transverse magnetization induces currents in the birdcage resonator and those currents rotate the magnetization in the z direction toward the x-y plane. The extra transverse magnetization has a different phase and causes broadening of the NMR lines. This effect is known as radiation damping and enters with a time constant $T_R=(2\pi\gamma M\eta_{\text{sphere}}Q_r)^{-1}$ in the equations of motion for the magnetization.[43] Here, η_{sphere} is a filling factor and Q_r the quality factor of the resonator. Each mode in the spectrum is only sensitive to radiation damping effects due to the mode itself, because the extra transverse magnetization induced by other modes has a different frequency and averages out to zero over sufficient precessions. Therefore, we take for η_{sphere} the filling factor of a spherical sample with a radius of 1 mm multiplied by the weight of a single mode. Our estimate—within a factor 2—of the increase of the half-width due to radiation damping is $\delta f_{\text{rad}}=0.025$ Hz for a weight of the first mode of 0.0016, $\eta_{\text{sphere}}=0.006$, $\gamma M_0=12.9$ rad/s, and $Q_r=200$. The broadening almost does not depend on the polarization enhancement factor, because the increase in $\gamma\mathcal{A}M_0$ is compensated by a decrease in the weight of the first mode: $\delta f_{\text{rad}}=0.030$ Hz for a weight of the first mode of 0.0006 at $\mathcal{A}=3$. All measured values for the half-width of the first mode $\delta f_{(0,0)}$ are in the range 1.2–3.4 Hz and the maximum correction for the values of $\lambda\mathcal{A}\omega_0\tau_\perp$ is an increase of 2.5%. We have applied a radiation damping correction by multiplying the data for $\lambda\mathcal{A}\omega_0\tau_\perp$ with $\delta f_{(0,0)}/(\delta f_{(0,0)}-\delta f_{\text{rad}})$ and $\delta f_{\text{rad}}=0.03$ Hz.

A validity check of the data analysis is that the results for γGR and $D_\perp/\lambda\omega_0\tau_\perp=\gamma GR(\xi/R)^3\mathcal{A}R^2$ must be constant. The experimental values for γGR and $D_\perp/\lambda\omega_0\tau_\perp$ averaged over all spectra are $\gamma GR=47\,270\pm355$ rad/s and $D_\perp/\lambda\omega_0\tau_\perp=0.015\,43\pm0.000\,33$ cm^2/s. The average value of γGR agrees within the error bars with the value for γGR calculated from the specifications of the gradient coil and the intrinsic gradient of the 12 T coil ($48\,230\pm2500$ rad/s). However, the spectra taken at the beginning of each experimental run where the polarization and temperature change rapidly ($1.5<\mathcal{A}<2.5$ as shown in Fig. 3) show some systematic deviations. The results of the spectra with $1.5<\mathcal{A}<2.5$ for $D_\perp/\lambda\omega_0\tau_\perp$ are about two standard deviations larger than the averaged value of $D_\perp/\lambda\omega_0\tau_\perp$ and for γGR about two standard deviations smaller than the averaged value of γGR. This may be related to a global phase shift of up to $\pi/6$ in those spectra with respect to the spectra obtained when the polarization is almost stationary.

The magnetization enhancement by dilution could be the origin for the phase shift and the slight variation in $D_\perp/\lambda\omega_0\tau_\perp$. The homogeneity of the z component of the magnetization in the cavity is worst for the data points with the largest rate of magnetization increase (the smallest magnetization enhancement factor). On the other hand, the tranverse spin currents after a rf pulse tend to homogenize the amplitude of the magnetization. Consequently, the establishment of the spin-wave spectrum after a rf pulse and the spectrum itself could be affected by a gradient in the longitudinal magnetization or by a longitudinal spin current.

Finally, the Leggett equations are valid[13] as long as the distance over which the quasiparticle distribution function changes (ξ) is greater than either the quasiparticle mean free path $l_\perp=v_F\tau_\perp$ or the spin rotation length $l_\perp/\lambda\mathcal{A}\omega_0\tau_\perp$. Our experiment meets this condition, since $\xi\geqslant20\ \mu$m and $l_\perp/\lambda\mathcal{A}\omega_0\tau_\perp\lesssim3D_\perp/v_F\lambda\omega_0\tau_\perp=0.16\ \mu$m.

V. RESULTS

We analyze the polarization and temperature dependence of the spectrum parameters $Q=\lambda\mathcal{A}\omega_0\tau_\perp$, ξ/R and γGR in two different ways to determine the anisotropy temperature T_{a0}. The first "direct" method allows us to obtain $\lambda\tau_\perp$ and T_{a0} from the relation

$$\frac{1}{\mathcal{A}Q}=\frac{1}{\omega_0C_\tau}\left(\frac{T^2}{\mathcal{A}^2}+T_{a0}^2\right) \tag{7}$$

and the second "indirect" method allows us to obtain $D_\perp$ and T_{a0} from an expression for $R^2/D_\perp$:

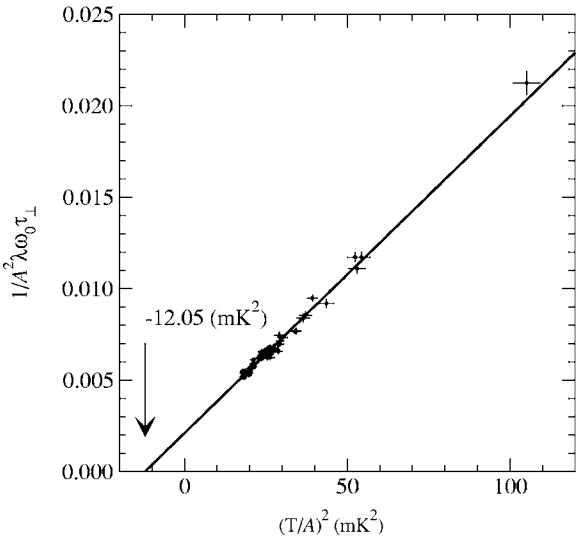

FIG. 6. The experimental results for $Q=\lambda\mathcal{A}\omega_0\tau_\perp$, $\mathcal{A}$, and T shown as $1/\mathcal{A}^2\lambda\omega_0\tau_\perp$ versus $(T/\mathcal{A})^2$.

$$\frac{1}{Q\gamma GR(\xi/R)^3} = \frac{R^2}{C_D}(T^2 + \mathcal{A}^2 T_{a0}^2). \tag{8}$$

Here, the constants C_τ and C_D are defined by the relations $\lambda\tau_\perp \equiv C_\tau/(T^2+\mathcal{A}^2T_{a0}^2)$ and $D_\perp \equiv C_D/(T^2+\mathcal{A}^2T_{a0}^2)$. Both methods should give the same value for T_{a0} if $D_\perp/\lambda\omega_0\tau_\perp$ is a constant.

The data have been taken in three experimental runs using different circulation rates to vary the conditions in the Leiden dilution refrigerator. Figures 6 and 7 show the data as $1/\mathcal{A}^2\lambda\omega_0\tau_\perp$ versus $(T/\mathcal{A})^2$ and $R^2/\mathcal{A}^2D_\perp$ versus $(T/\mathcal{A})^2$. The error bars have been calculated from the estimated errors in temperature, polarization enhancement factor, and spectrum parameters: (1) the errors in the temperature have been estimated from the scatter to be 2%, (2) the errors in the polarization enhancement factor $\mathcal{A}$ for each point have been estimated to be 1% from the difference between the

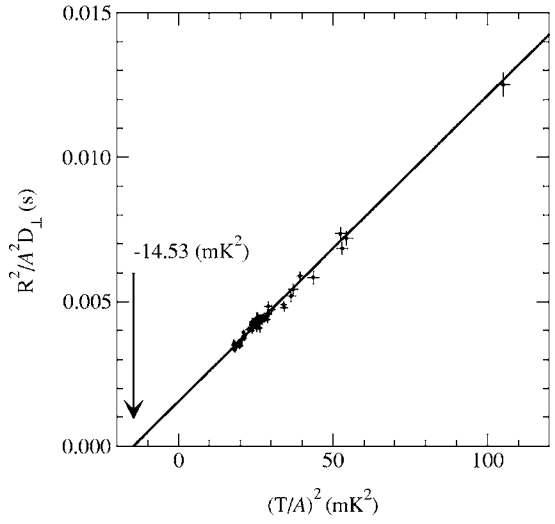

FIG. 7. The experimental results for $Q=\lambda\mathcal{A}\omega_0\tau_\perp$, γGR, ξ/R, $\mathcal{A}$, and T shown as $R^2/\mathcal{A}^2D_\perp$ versus $(T/\mathcal{A})^2$.

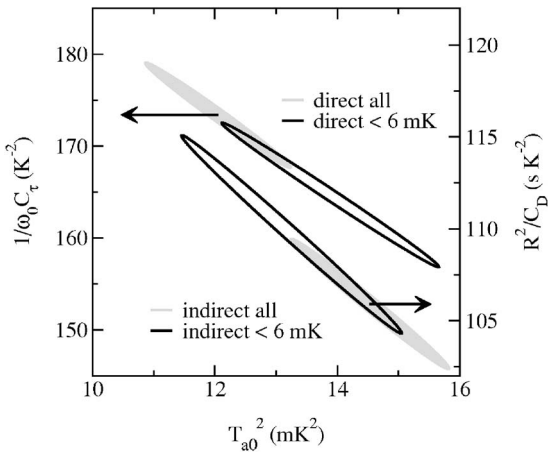

FIG. 8. The 68% confidence regions for the direct (the two upper ellipses) and indirect (the two lower ellipses) methods using all spectra (the ellipses drawn with a full line) or the spectra with $T/\mathcal{A}<6$ mK (the gray ellipses).

continuous-wave NMR frequency up- and downsweeps used to measure the polarization, and (3) the errors in $\lambda\mathcal{A}\omega_0\tau_\perp$, ξ/R, and γGR (typically 2%, 1%, and 0.1%) are the statistical errors given by the analysis of each spectrum. The vertical and horizontal error bars in Figs. 6 and 7 are correlated because the errors in both directions have a contribution from the error in the polarization enhancement factor. We have applied an orthogonal distance regression method to fit the data in Fig. 6 with Eq. (7), where we have accounted for the correlation between the horizontal and vertical error bars. The orthogonal distance regression of the data in Fig. 7 using Eq. (8) has the advantage of uncorrelated error bars. The straight lines in Figs. 6 and 7 have been calculated from the fits to all spectra represented in the figures.

We recall that our experimental values of the ratio $D_\perp/\lambda\omega_0\tau_\perp$ are not quite constant for the spectra with $1.5<\mathcal{A}<2.5$. To investigate the consequences of the systematic deviation we have also analyzed the data selecting the spectra with $T/\mathcal{A}<6$ mK to exclude the 10% of the data showing the largest systematic error. Figure 8 shows the four 68% confidence regions of the results from the analysis of the two data sets with the direct and indirect method. There is excellent agreement between the results for T_{a0}^2 obtained with the direct and indirect method if we restrict the analysis to data with $T/\mathcal{A}<6$ mK. The agreement between the results for T_{a0}^2 obtained by both methods is somewhat less satisfactory without the selection, but the average value of T_{a0}^2 does not change when we include the data points with $T/\mathcal{A}>6$ mK.

Table I shows the values obtained by the direct and indirect method including the radiation damping correction. The correction decreases the results for T_{a0}^2, C_τ, and C_D by about half a standard deviation.

An advantage of our data analysis is that the results for C_τ and C_D do not depend on a calibration of the field gradient, because γGR results from the fits to the spectra. The 5% uncertainty in the radius of the cavity introduces an additional 10% uncertainty in the values for C_D. Presently, we are unable to evaluate the consequences of a nonuniform field

TABLE I. The results of the analysis using the direct and indirect methods. In addition to the statistical uncertainties in this table, there is an uncertainty of 10% in C_D due to the uncertainty of 5% in R.

	Direct method	
Data set	T_{a0}^2 (mK^2)	C_τ (10^{-12} s K^2)
All	12.05±0.78	2.492±0.054
$T/\mathcal{A}<6$ mK	13.88±1.17	2.623±0.083
	Indirect method	
Data set	T_{a0}^2 (mK^2)	C_D (10^{-6} cm^2 s^{-1} K^2)
All	14.53±0.85	94.4±2.1
$T/\mathcal{A}<6$ mK	13.25±1.19	91.2±3.0

gradient or a deformation of the hemispherical shape of the cavity.

Our results for C_D and C_τ in a saturated 9.4% mixture at 8 bars can be compared with some of the results published by Ishimoto *et al.*[44] at frequencies of 1 and 2 MHz in an 8.6% mixture at 8 bars. We find $D_\perp/\lambda\tau_\perp=C_D/C_\tau=(37.9\pm4.2)\times10^6$ cm^2 s^{-2} for the data set with $T/\mathcal{A}<6$ mK. This agrees within the combined error bars with the value $D_\perp/\lambda\tau_\perp=(43\pm3)\times10^6$ cm^2 s^{-2} obtained by Ishimoto *et al.*[44] from the frequency distance between spin-wave modes. They did not measure $\tau_\perp$ or $\lambda\tau_\perp$,[44] but calculated $\tau_\perp$ from measurements of the spin diffusion constant published by Murdock *et al.*[45] Our spin diffusion result $C_D=(91\pm10)\times10^6$ cm^2 K^2/s is too high in comparison with the extrapolation $C_D=(63\pm6)\times10^6$ cm^2 K^2/s from Fig. 4 by Murdock *et al.* However, other spin diffusion experiments[16,20,46,47] at 0 bar indicate that the results by Murdock *et al.* may be 10–20 % too low.

VI. DISCUSSION AND CONCLUSION

Finally, we present the statistical average of the values for T_{a0}^2 in Table I as our main result: $T_{a0}^2=13.43\pm1.06$ mK^2 or $T_{a0}=3.66\pm0.14$ mK. This result is consistent with the prediction that transverse spin transport relaxes in the zero-temperature limit. Our value for T_{a0} is 30% higher than the theoretical prediction for very dilute mixtures $T_{a0}=2.815$ mK and confirms the result of the spin-echo experiment by Akimoto *et al.*[20] A significant difference between the two experiments is the value of λ which almost crosses zero at the critical concentration $x_3=x_c$ in the spin-echo experiment. Meyerovich and Musaelian[3] have suggested that the spin dynamics may be modified at x_c, but no evidence of this has been observed.[20]

Our result is significantly lower than the value $T_{a0}=6.1\pm1$ mK obtained by Buu *et al.*[19] in a 6.2% mixture at 0 bar in a magnetic field of 11.3 T. However, those authors did not address the question of why their measurement of the spin diffusion coefficient resulted in $C_D=(22\pm5)\times10^6$ cm^2 K^2/s, a factor 3–4 lower than expected. Our experiment improves in two aspects on the previous spin-wave experiment[22] which did not have the sensitivity to distinguish between the dilute Fermi gas prediction and $T_{a0}=0$ K: the thermometry based on vibrating wire viscometry and the internal consistency of the analysis. The temperature dependence of the viscosity in the earlier experiment was approximated by a semiphenomenological interpolation of data[22,35,48] in disagreement with the calibration discussed in Sec. III. Moreover, the analysis of viscometer data in the earlier experiment did not account for the slip effects mentioned in Sec. III, but posterior inspection of the data revealed the presence of slip effects. In addition, the final result for T_{a0} in the earlier experiment depended on extrapolated values for C_D and C_τ.[22,44] The discrepancy with the present spin wave experiment would be resolved when the

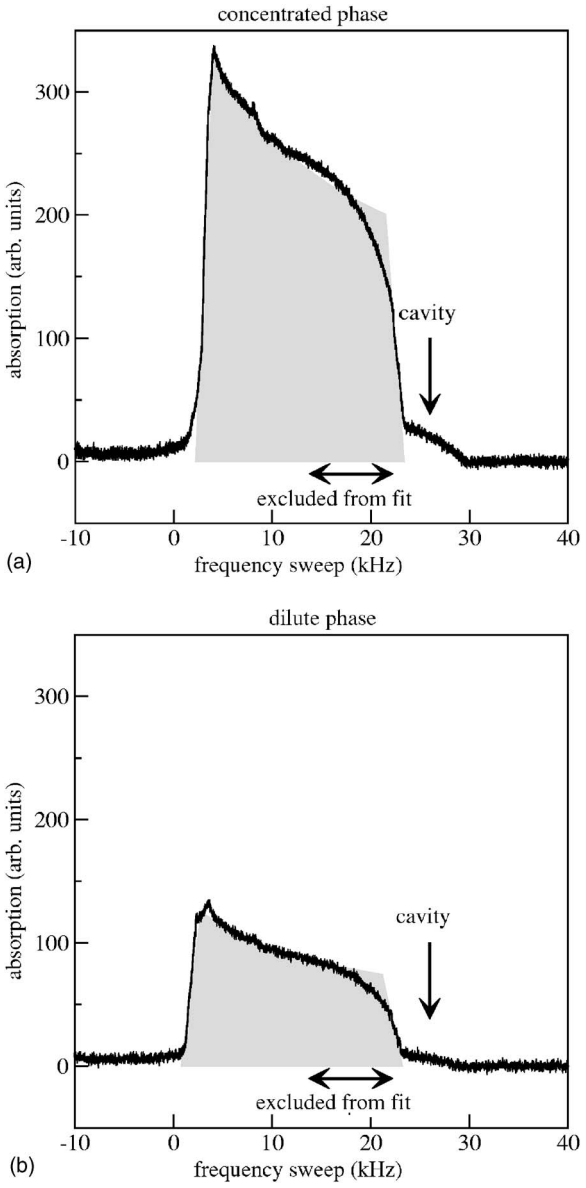

FIG. 9. Comparison of the experimental NMR lines of the mixing chamber filled with dilute and concentrated phase with fits of the line shape of a cylinder with a height of 3 mm and a diameter of 5 mm in a field profile of the form (A1). The rounding of the experimental lines in the region from 14 to 22 kHz is due to a meniscus of epoxy. This region has been excluded from the fits.

real value for C_τ at 7 bars would be closer to our present result $C_\tau=(2.623\pm0.083)\times10^{-12}$ s K^2 at 8 bars than the extrapolation $C_\tau=(1.8\pm0.2)\times10^{-12}$ s K^2 used in the analysis of the previous spin wave experiment.

Meyerovich and Musaelian[3] have used an argument based on a Mathiessen-type rule to derive the effect of the interactions on the anisotropy temperate. They find

$$T_{a0}=\frac{\hbar\gamma B_0}{2\pi k_B}\sqrt{2C_D}\left(\frac{a_H}{a_T}\frac{\sqrt{1+2F_0^a-F_1^a/3}}{(1+F_0^a)(1+F_1^a/3)}\right),$$

where $\sqrt{2C_D}\approx1.26$, and a_H and a_T are two related scattering lengths resulting from different angular averages of the the same particle scattering probability. The Landau parameters are all much smaller than 1, so in this context our value for T_{a0} is compatible with $a_H/a_T\approx1$ in a 9.4% mixture.

ACKNOWLEDGMENTS

We thank P. J. Nacher for questioning us on the importance of the dipolar interactions and radiation damping.

APPENDIX: THE MAGNETIC FIELD PROFILE

The shape of the NMR spectra at the maximum field gradient of the experimental chamber filled with concentrated and dilute phase in Fig. 9 also shows that the field gradient is nonuniform. We have assumed that the static field is of the form

$$B_z(z,r)=B_0+g_1z+g_2\left(z^2-\frac{r^2}{2}\right) \tag{A1}$$

to evaluate the deviations from a uniform gradient. Equation (A1) is the most general Taylor expansion of the field up to second order under the assumption of rotational symmetry about the vertical z axis. Figure 9 compares the fits of the line shape based on Eq. (A1) for a cylinder with a height of 3 mm and a diameter of 5 mm with the experimental line shape of the mixing chamber filled with concentrated and dilute phase. We find $g_1=20.1$ G/cm and $g_2=18.3$ G/cm^2 for the concentrated phase and $g_1=21.2$ G/cm and $g_2=20.4$ G/cm^2 for the dilute phase. We believe that the values for g_2 are overestimated, because the line shape depends also on field shimming in the x and y directions. The optimal current in the shim coils depend on the applied gradient in the z direction. We did not shim the field for each g_1, since the spin-wave spectra in the cavity are almost insensitive to field shimming.

*Electronic address: gerard.vermeulen@grenoble.cnrs.fr

[1] A. E. Meyerovich, Phys. Lett. **107A**, 177 (1985).
[2] W. J. Mullin and J. W. Jeon, J. Low Temp. Phys. **88**, 433 (1992).
[3] A. E. Meyerovich and K. A. Musaelian, Phys. Rev. Lett. **72**, 1710 (1994).
[4] D. I. Golosov and A. E. Ruckenstein, Phys. Rev. Lett. **74**, 1613 (1995).
[5] J. W. Jeon, Ph.D. thesis, University of Massachusetts, 1989.
[6] D. I. Golosov and A. E. Ruckenstein, J. Low Temp. Phys. **112**, 265 1998.
[7] I. A. Fomin, JETP Lett. **65**, 749 (1997).
[8] W. J. Mullin and R. J. Ragan, J. Low Temp. Phys. **138**, 73 (2005).
[9] I. A. Fomin (private communication).
[10] V. P. Mineev, Phys. Rev. B **72**, 144418 (2005).
[11] A. E. Meyerovich and K. A. Musaelian, J. Low Temp. Phys. **89**, 781 (1992).
[12] J. W. Jeon and W. J. Mullin, Phys. Rev. Lett. **62**, 2691 (1989).
[13] A. J. Leggett, J. Phys. C **3**, 448 (1970).
[14] L.-J. Wei, N. Kalechofsky, and D. Candela, Phys. Rev. Lett. **71**, 879 (1993).
[15] D. Candela, H. Akimoto, R. M. Bowley, O. Buu, D. Clubb, and J. R. Owers-Bradley, J. Low Temp. Phys. **121**, 767 (2000).
[16] J. H. Ager, A. Child, R. König, J. R. Owers-Bradley, and R. M. Bowley, J. Low Temp. Phys. **99**, 683 (1995).
[17] J. R. Owers-Bradley, R. M. Bowley, O. Buu, D. Clubb, and G. Vermeulen, J. Low Temp. Phys. **121**, 779 (2000).
[18] H. Akimoto, J. Xia, E. Adams, D. Candela, W. Mullin, and N. S. Sullivan, J. Low Temp. Phys. **126**, 109 (2002).
[19] O. Buu, D. Clubb, R. Nyman, J. R. Owers-Bradley, and R. König, J. Low Temp. Phys. **128**, 123 (2002).
[20] H. Akimoto, D. Candela, J. S. Xia, W. J. Mullin, E. D. Adams, and N. S. Sullivan, Phys. Rev. Lett. **90**, 105301 (2003).
[21] O. Buu, R. Nyman, R. M. Bowley, and J. R. Owers-Bradley, Phys. Rev. B **65**, 134512 (2002).
[22] G. Vermeulen and A. Roni, Phys. Rev. Lett. **86**, 248 (2001).
[23] D. Candela, D. R. McAllaster, and L.-J. Wei, Phys. Rev. B **44**, 7510 (1991).
[24] V. P. Mineev, Phys. Rev. B **69**, 144429 (2004).
[25] A. Meyerovich, in *Helium Three*, edited by W. P. Halperin and L. P. Pitaevskii (Elsevier, Amsterdam, 1990), p. 757.
[26] P. L. Krotkov, V. P. Mineev, and G. A. Vermeulen, Phys. Rev. B **65**, 054301 (2002).
[27] L. R. Walker, Phys. Rev. **105**, 390 (1957).
[28] E. Stoltz, J. Tannenhauser, and P. J. Nacher, J. Low Temp. Phys. **101**, 839 (1995).
[29] J. Jeener, Phys. Rev. Lett. **82**, 1772 (1999).
[30] The result for T_{a0} including the dipolar field correction is 10% lower than the result for T_{a0} without those corrections.
[31] A. Rodrigues and G. Vermeulen, J. Low Temp. Phys. **108**, 103 (1997).
[32] S. Perisanu and G. Vermeulen, J. Low Temp. Phys. **134**, 701 (2004).
[33] R. M. Bowley and J. R. Owers-Bradley, J. Low Temp. Phys. **136**, 15 (2004).
[34] S. Perisanu and G. Vermeulen, J. Low Temp. Phys. **138**, 19 (2005).
[35] J. C. H. Zeegers, A. T. A. M. de Waele, and H. M. Gijsman, J. Low Temp. Phys. **84**, 37 (1991).
[36] K. S. Dy and C. J. Pethick, Phys. Rev. **185**, 373 (1969).
[37] S. Perisanu and G. Vermeulen, Phys. Rev. B **73**, 134517 (2006).
[38] G. A. Vermeulen, A. Schuhl, F. B. Rasmussen, J. Joffrin, G.

Frossati, and M. Chapellier, Phys. Rev. Lett. **60**, 2315 (1988).
[39] O. Buu, A. C. Forbes, L. Puech, and P. E. Wolf, Phys. Rev. Lett. **83**, 3466 (1999).
[40] C. A. M. Castelijns, J. G. M. Kuerten, A. T. A. M. de Waele, and H. M. Gijsman, Phys. Rev. B **32**, 2870 (1985).
[41] J. G. M. Kuerten, C. A. M. Castelijns, A. T. A. M. de Waele, and H. M. Gijsman, Cryogenics **25**, 419 (1985).
[42] H. Akimoto and D. Candela, J. Low Temp. Phys. **121**, 791 (2000).
[43] N. Bloembergen and R. V. Pound, Phys. Rev. **95**, 8 (1954).
[44] H. Ishimoto, H. Fukuyama, T. Fukuda, T. Tazaki, and S. Ogawa, Phys. Rev. B **38**, 6422 (1988).
[45] E. Murdock, K. Mountfield, and L. Corruccini, J. Low Temp. Phys. **31**, 581 (1978).
[46] A. C. Anderson, D. O. Edwards, W. R. Roach, R. E. Sarwinski, and J. C. Wheatley, Phys. Rev. Lett. **17**, 367 (1966).
[47] H. Akimoto, O. Ishikawa, G.-H. Oh, M. Nakagawa, T. Hata, and T. Kodama, J. Low Temp. Phys. **82**, 295 (1991).
[48] R. König and F. Pobell, J. Low Temp. Phys. **97**, 287 (1994).